










ATMOSPHERIC RADIOCARBON FOR THE PERIOD 1950–2019

Quan Hua^{1*}  • Jocelyn C Turnbull^{2,3}  • Guaciara M Santos⁴  • Andrzej Z Rakowski⁵ • Santiago Ancapichún^{6,7}  • Ricardo De Pol-Holz⁷  • Samuel Hammer⁸ • Scott J Lehman⁹ • Ingeborg Levin⁸  • John B Miller¹⁰  • Jonathan G Palmer^{11,12}  • Chris S M Turney^{11,12} 

¹Australian Nuclear Science and Technology Organisation, Locked Bag 2001, Kirrawee DC, NSW 2232, Australia

²Rafter Radiocarbon Laboratory, GNS Science, Lower Hutt, New Zealand

³CIRES, University of Colorado, Boulder, CO, USA

⁴Earth System Science, University of California, Irvine, B321 Croul Hall, Irvine, CA 92697-3100, USA

⁵Institute of Physics, Center for Science and Education, Silesian University of Technology, 44–100 Gliwice, Poland

⁶Postgraduate School in Oceanography, Faculty of Natural and Oceanographic Sciences, Universidad de Concepción, Concepción, Chile

⁷Centro de Investigación GAIA Antártica (CIGA) and Network for Extreme Environment Research (NEXER), Universidad de Magallanes, Punta Arenas, Chile

⁸Institut für Umweltphysik, Heidelberg University, INF 229, 69120 Heidelberg, Germany

⁹INSTAAR, University of Colorado, Boulder, CO 80309-0450, USA

¹⁰NOAA Global Monitoring Laboratory, Boulder, CO 80305, USA

¹¹ARC Centre of Excellence for Australian Biodiversity and Heritage, School of Biological, Earth and Environmental Sciences, University of New South Wales, NSW 2052, Australia

¹²Chronos ¹⁴Carbon-Cycle Facility and the Earth and Sustainability Science Research Centre, University of New South Wales, NSW 2052, Australia

ABSTRACT. This paper presents a compilation of atmospheric radiocarbon for the period 1950–2019, derived from atmospheric CO₂ sampling and tree rings from clean-air sites. Following the approach taken by Hua et al. (2013), our revised and extended compilation consists of zonal, hemispheric and global radiocarbon (¹⁴C) data sets, with monthly data sets for 5 zones (Northern Hemisphere zones 1, 2, and 3, and Southern Hemisphere zones 3 and 1–2). Our new compilation includes smooth curves for zonal data sets that are more suitable for dating applications than the previous approach based on simple averaging. Our new radiocarbon dataset is intended to help facilitate the use of atmospheric bomb ¹⁴C in carbon cycle studies and to accommodate increasing demand for accurate dating of recent (post-1950) terrestrial samples.

KEYWORDS: Anthropocene, atmospheric carbon dioxide, bomb peak, bomb radiocarbon, the global carbon cycle, tree rings.

INTRODUCTION

Radiocarbon or ¹⁴C is naturally produced in the upper atmosphere by the interaction of the secondary neutron flux from cosmic rays with atmospheric nitrogen-14 (¹⁴N; Libby 1952). Following its production and oxidation to carbon dioxide (CO₂), ¹⁴C enters the biosphere and oceans via photosynthesis and air-sea gas exchange, respectively, providing a supply of ¹⁴C that approximately compensates for the decay of the existing ¹⁴C in terrestrial and marine reservoirs. The resultant near steady state provides the basis for the traditional radiocarbon dating ca. 50,000 years back before 1950.

Radiocarbon is also produced anthropogenically. Atmospheric nuclear weapon testing mostly in the late 1950s and early 1960s produced large fluxes of thermal neutrons, which reacted with atmospheric ¹⁴N to form ¹⁴C (Libby 1956; Rafter and Fergusson 1957). The excess ¹⁴C produced by atmospheric nuclear detonations or so-called bomb ¹⁴C was mostly injected into the stratosphere and subsequently transported to the troposphere, which together with ¹⁴C-free fossil-fuel emissions, atmospheric circulation patterns and rapid exchanges between the global carbon reservoirs shaped the tropospheric $\Delta^{14}\text{C}$ levels during the past ca. 70 years. We note that $\Delta^{14}\text{C}$ used in this paper is the fractionation- and age-corrected

*Corresponding author. Email: ghx@ansto.gov.au

deviation from the standard pre-industrial ^{14}C content in atmospheric CO_2 , which is the Δ term of Stuiver and Polach (1977). Atmospheric $\Delta^{14}\text{CO}_2$ (or atmospheric $\Delta^{14}\text{C}$ in short) followed a decreasing trend from ca. 1900 due to the Suess effect (Suess 1955), started increasing in 1955, then reached its maximum levels in 1963–1964 in the Northern Hemisphere (NH) and 1964–1965 in the Southern Hemisphere (SH), and has decreased approximately exponentially since then (e.g., Levin and Heshshaimer 2000; Hua et al. 2003; Turney et al. 2018). Rapid exchange between the atmosphere, and the terrestrial biosphere and oceans resulted in substantial decreases in atmospheric $\Delta^{14}\text{C}$ and increases in $\Delta^{14}\text{C}$ of the surface ocean during the mid-1960s to mid-1980s, allowing the use of bomb ^{14}C to study air-sea exchange of CO_2 , ocean circulation, and the global carbon cycle (Nydal 1968; Oeschger et al. 1975; Druffel and Suess 1983; Levin and Heshshaimer 2000; Randerson et al. 2002; Hua et al. 2003; Key et al. 2004; Krakauer et al. 2006; Naegler 2009; Levin et al. 2010). Large differences in atmospheric $\Delta^{14}\text{C}$ levels during the post-1955 period also enable the use of bomb ^{14}C as a powerful dating tool, which can deliver dating accuracies of one to a few years for recent terrestrial samples (Hua and Barbetti 2004).

Several compilations of recent atmospheric $\Delta^{14}\text{C}$ for use in carbon cycle modeling and/or age calibration have been carried out previously. Based on a small number of atmospheric, tree-ring and organic samples, Tans (1981) performed the earliest compilation of recent atmospheric $\Delta^{14}\text{C}$ for the period 1954–1977 for use in carbon cycle model calculations. Recently, Graven et al. (2017) created annual atmospheric $\Delta^{14}\text{C}$ datasets for 3 regions (NH north of 30°N , tropics between 30°N – 30°S and SH south of 30°S) for the period 1850–2015 for use in the Coupled Model Intercomparison Project 6 (CMIP6). For the period 1950–2015, this compilation was derived from tree-ring $\Delta^{14}\text{C}$ data and a large number of atmospheric $\Delta^{14}\text{C}$ records. Goodsite et al. (2001) brought together recent atmospheric $\Delta^{14}\text{C}$ for the NH for use in ^{14}C dating of their peat cores from Denmark. This atmospheric $\Delta^{14}\text{C}$ curve was based on a limited number of atmospheric sampling, tree-ring records and organic samples north of 27°N during 1950–1998. In addition, Hua and Barbetti (2004) compiled summer and monthly atmospheric $\Delta^{14}\text{C}$ data for the period 1955–2001 for use in carbon cycle modeling and ^{14}C dating, respectively. The authors defined zonal distributions of bomb $\Delta^{14}\text{C}$ (3 zones in the NH and 1 zone for the SH) during the bomb peak period, reflecting major zones of atmospheric circulation. This compilation, derived from a large number of atmospheric and tree-ring records and measurement of organic materials, provided zonal, hemispheric and global summer $\Delta^{14}\text{C}$ data sets, and 4 zonal data sets with (mostly) monthly resolution. Hua et al. (2013) subsequently defined another zone for the SH, increasing the number of discrete atmospheric zones from 4 to 5. They refined the dataset of Hua and Barbetti (2004), resulting in compiled summer and (mostly) monthly $\Delta^{14}\text{C}$ data sets for 1950–2011.

In this paper, we present a new compilation of atmospheric $\Delta^{14}\text{C}$ for the period 1950–2019, which is an extended and revised version of the compilation of Hua et al. (2013) with the addition of recent data from 4 atmospheric sampling records and 11 new tree-ring records. We provide two datasets, one for summertime and the other with monthly resolution for each year of record. The compiled zonal, hemispheric and global summer data are intended for use in carbon cycle model calculations, while zonal monthly data were constructed to facilitate the dating of recent organic materials. We also incorporate curve fitting to smooth the data and make it more appropriate for dating applications, because this method delivers continuous datasets with suppressed outliers and clear seasonal cycles for the periods covered by atmospheric $\Delta^{14}\text{C}$ records.

DATA SETS USED FOR THE COMPILATION

Selection Criteria

The current compilation is based on representative radiocarbon measurement series from tree rings and direct atmospheric CO_2 sampling from clean-air sites and rural areas, which are not strongly affected by local fossil-fuel emissions or nuclear facilities. This primary data selection criterion is similar to that adopted by Hua and Barbetti (2004) and Hua et al. (2013).

For tree rings, two additional selection criteria were employed. One of them is on tree-ring chronologies to ensure that selected tree rings are properly dated. This criterion involves tree-ring dating by (i) using the dendrochronological method of cross-dating, which is comprised of multiple trees and often multiple tree radii or tree cores per tree collected, measured and their ring-widths pattern matched from the same location (e.g., Speer 2010), or (ii) ring counting within the sample by applying a similar type of dendro-analytical process to match ring-width variations within two or more tree radii. The other criterion relates to tree-ring pretreatment for radiocarbon analysis. Only tree rings with sufficient pretreatment to remove non-structural carbon (NSC) compounds (Carbone et al. 2013), and extract holocellulose or alpha-cellulose, which mostly reflects atmospheric $\Delta^{14}\text{C}$ at the time of tree growth, were selected for analysis.

Atmospheric CO_2 Sampling

Atmospheric $\Delta^{14}\text{C}$ data sets selected for the study include those used in Hua et al. (2013) and recent data from Schauinsland (Germany; 47°55'N, 7°55'E; 2004–2016; Hammer and Levin 2017), Jungfraujoch (Switzerland; 46°33'N, 7°42'E; 2004–2019; Hammer and Levin 2017; Emmenegger et al. 2020), Niwot Ridge (USA; 40.05°N, 105.58°W; 2007–2018; Lehman et al. 2013; Lehman and Miller 2019), and Wellington (New Zealand; 41°S, 175°E; 2012–2019; Turnbull et al. 2017). Revisions of the Wellington data for the periods 1990–1993 and 1995–2005, reported in Turnbull et al. (2017), were also incorporated into this compilation.

As there are strong influences of fossil-fuel combustion in winters for Kasprowy Wierch from Poland (49°N, 20°E) in Central Europe (Zimnoch et al. 2012), only the summer $\Delta^{14}\text{C}$ data from this record was included in Hua et al. (2013). Because this record is quite short, spanning only 2008–2009, and there are now 2 additional data sets from Central Europe (Schauinsland and Jungfraujoch), the decision was made to exclude the Kasprowy Wierch data set from the current study.

Tree Rings

Our study employs 22 tree-ring records, consisting of 11 from Hua et al. (2013) and 11 new ones. Four tree-ring data sets employed in Hua et al. (2013) were omitted from our compilation as they failed to satisfy our selection criteria. The Kiel record (Germany; 54°N, 10°E; 1955–1964) is one of the rejected series because there was no supporting information on the tree-ring dating (Willkomm and Erlenkeuser 1968) and our pretreatment criterion was not satisfied (only acid-alkali-acid (AAA) pretreatment was used; H. Erlenkeuser, personal communication June 2020). The other three data sets all failed the tree-ring pretreatment criterion. They include Gifu (Japan; 36°N, 138°E; 1955–1959; Nakamura et al. 1987a, 1987b) and Saigon (Vietnam; 11°N, 107°E; 1962, 1964–1967; Kikata et al. 1992, 1993) using the AAA pretreatment method, and Agematsu (Japan; 36°N, 138°E; 1960–1967, 1969) using Soxhlet solvent extraction followed by AAA (Muraki et al. 1998).

Recently published tree-ring ^{14}C data sets included in our compilation are Scots pine (*Pinus sylvestris*) from central Norway (63°16'N, 10°27'E, 1953–1965; Svarva et al. 2019), oak (*Quercus borealis*) from Eastern Jutland, Denmark (56°11'N, 10°13'E; 1954–1970; Kudsk et al. 2018), white oak (*Quercus garryana*) from western Oregon, USA (45°07'N, 123°27'W; 1950–1952 and 1960–1969; Cain et al. 2018), Douglas fir (*Pseudotsuga menziesii*) from northeastern Mexico (23°49'N, 99°50'W; 1950–2002; Beramendi-Orosco et al. 2018), Japanese cedar (*Cryptomeria japonica*) from Fukushima, Japan (37.01°N, 140.81°E; 1984–1994; Xu et al. 2015), *Polylepis tarapacana* from Irruputuncu, Altiplano, Chile (22°S, 68°W; 1950–2014; Ancapichún et al. 2021), *Araucaria angustifolia* from Camanducaia, Brazil (22°50'S, 46°04'W; 1927–1997; Santos et al. 2015), *Pinus radiata* and *Agathis australis* from Wellington, New Zealand (41°S, 175°E; 1950–2011; Turnbull et al. 2017), and *Dracophyllum* spp. from Campbell Island, New Zealand (52.554°S, 169.133°E; 1953–2011; Turney et al. 2018).

Two data sets on oak (*Quercus borealis*) from Uppsala, Sweden (60°00'N, 17°38'E; 1951–1967 and 1980–1981; Olsson and Possnert 1992) and Sitka spruce (*Picea sitchensis*) from Washington state, USA (47°57'N, 124°33'W; 1962–1964; Grootes et al. 1989), which were inadvertently omitted from the previous compilations (Hua and Barbetti 2004; Hua et al. 2013), are now also included in the current study. The Washington Sitka spruce sub-annual tree-ring samples have recently been remeasured at the National Laboratory for Age Determination in Trondheim. These new, unpublished $\Delta^{14}\text{C}$ results are similar to those published in Grootes et al. (1989) but have much higher precision (H. Svarva, M.-J. Nadeau, and P. Grootes, personal communication July 2020). We, therefore, used these new data instead of the published original data for our compilation.

Kudsk et al. (2018) compared $\Delta^{14}\text{C}$ of earlywood (EW) and latewood (LW) of their Danish oak (1954–1970) record and the Swedish oak record (1951–1967 and 1980–1981) of Olsson and Possnert (1992) with the compiled monthly NH zone 1 data of Hua et al. (2013) derived from atmospheric sampling (1959–2009). They reported that the LW fraction of the two records formed in June–July (mid-summer), while the EW fraction of the Danish and Swedish records contained carbon assimilated in spring and probably from the previous year, respectively. As the timing of the LW formation is similar to that of tree-ring growth seasons (see later discussion), only the LW ^{14}C data of these two oak records were included in the compilation.

Xu et al. (2015) measured ^{14}C in EW, LW and (whole) annual rings of a Japanese cedar located ca. 50 km southwest of the Fukushima Dai-ichi Nuclear Power Plant during the period 1984–2013 to see whether there was a significant release of anthropogenic ^{14}C from the power plant accident in 2011. Only the tree-ring ^{14}C data for the period before the accident, which agree well with the compiled NH zone 2 data of Hua et al. (2013), are included here. To be consistent, the data of the whole ring in 1994 and LW fraction from 1984 to 1989 were used although $\Delta^{14}\text{C}$ values of these LW samples and their associated EW samples are similar.

For the sub-annual Norwegian tree-ring record (8 incremental samples per year) of Svarva et al. (2019), the first and last increments of each annual tree ring were excluded from our analyses. This is because of the possibility of cross-ring-boundary sampling resulting in unreliable $\Delta^{14}\text{C}$ values, especially for the bomb peak period (Svarva et al. 2019).

All atmospheric and tree-ring ^{14}C records used for our compilation are shown in Table 1 and illustrated in Figure 1.

Table 1 Atmospheric and tree-ring $\Delta^{14}\text{C}$ records used for the compilation of summer and monthly data sets.

PERIOD 1950–1972	
NH zone 1	NH zone 3
<i>Atmospheric sampling</i>	<i>Atmospheric sampling</i>
Fruholmen (71°06'N, 23°59'E; 1962–1972), Trondheim (63°16'–25°N, 10°15'–22°E; 1962–1963) and Lindesnes (57°59'N, 7°04'E; 1963–1964), Norway [1]	Debre Zeit, Ethiopia (8°40'N, 38°58'E; 1963–1969) [1]
Vermunt, Austria (47°4'N, 9°34'E; 1959–1972) [2]	<i>Tree rings</i>
China Lake, California, USA (35°32'N, 117°41'W; 1963–1968) [3]	Mandla, India (23°N, 81°E; 1955–1970) [16]
<i>Tree rings</i>	Doi Inthanon, Thailand (18°33'N, 98°34'E; 1950–1972) [17–18]
Trøndelag, Norway (63°16'N, 10°27'E; 1953–1965) [4]	SH zone 3
Uppsala, Sweden (60°0'N, 17°38'E; 1951–1956 & 1962–1967) [5]	<i>Tree rings</i>
Eastern Jutland, Denmark (56°11'N, 10°13'E; 1954–1970) [6]	Muna Is., Indonesia (5°S, 122°E; 1950–1972) [19]
Niepolomice, Poland (50°2'N, 20°13'E; 1960–1972) [7]	SH zone 1–2
Washington state, USA (48°N, 124°W; 1950–1954) [8] and (47°57'N, 124°33'W; 1962–1964) [9]	<i>Atmospheric sampling</i>
NE Hungary (47°35'N, 21°35'E; 1951–1972) [10]	Funatufi, Tuvalu (8.5°S, 179.2°E; 1966–1972) [20]
NH zone 2	Suva, Fiji (18.1°S, 178.4°E; 1958–1972) [20]
<i>Atmospheric sampling</i>	Fianarantsoa, Madagascar (21°27'S, 47°05'E; 1964–1972) [1]
Santiago de Compostela (42°53'N, 8°26'W; 1963–1966), Izaña (28°22'N, 16°30'W; 1963–1967) and Mas Palomas (27°45'N, 15°40'W; 1963–1972), Spain [1]	Pretoria, South Africa (25°43'S, 28°21'E; 1950–1972) [21]
Rehovot, Israel (31°50'N, 34°50'E; 1967–1968) [1]	Wellington (41.25–41°S, 174.69–87°E; 1954–1972) [22] and
Dakar, Senegal (14°33'–41'N, 17°07'–28°W; 1963–1968) [1]	Campbell Is (52.5°S, 169.2°E; 1970–1972) [20], New Zealand
<i>Tree rings</i>	Scott Base, Antarctica (77.9°S, 166.7°E; 1961–1972) [20]
W. Oregon (45°07'N, 123°27'W; 1950–1952 & 1960–1969) [11],	<i>Tree rings</i>
S. Arizona (32°26'N, 110°47'W; 1950–1955) [12], USA	Irruputuncu, Altiplano, Chile (20°S, 68°W; 1950–1972) [23]
NE Mexico (23°49'N, 99°50'W; 1950–1972) [13]	Camanducaia, Brazil (22°50'S, 46°04'W; 1950–1972) [24]
Shika-machi, Japan (37.1°N, 136.5°E; 1950–1972) [14]	Armidade (30°S, 152°E; 1953–1972) [25] and Tasmania (41°41'S, 145°18'E; 1953–1972) [17], Australia
Mts Chiak and Kyeryon, South Korea (37°20'–23'N, 128°03'–04'E; 1950–1970) [15]	Wellington (41.25–33°S, 174.87°E; 1951–1972) [22] and
	Campbell Is. (52.554°S, 169.133°E; 1953–1972) [26], New Zealand
PERIOD 1973–2019	
NH (NH zones 1, 2 and 3)	SH (SH zones 3 and 1–2)
<i>Atmospheric records</i>	<i>Atmospheric records</i>
Fruholmen, Norway (71°06'N, 23°59'E; 1973–1993) [1]	Cape Matatula, American Samoa (14.25°S, 170.57°W; 2001–2007) [31]
Point Barrow (Alaska; 71.38°N, 156.47°W; 1985–1991 [27] & 1999–2007 [28]), Niwot Ridge (Colorado; 40.05°N, 105.58°W; 2003–2018) [29], China Lake (California; 35°32'N, 117°41'W; 1977–1983) [30], and Kumukahi and Mauna Loa (Hawaii; 19.52–53°N, 154.82–155.58°W; 2001–2007) [31], USA	Suva, Fiji (18.1°S, 178.4°E; 1973–1975) [20]
Vermunt, Austria (47°4'N, 9°34'E; 1973–1986) [2]	Fianarantsoa, Madagascar (21°27'S, 47°05'E; 1973–1978) [1]
Schauinsland, Germany (47°55'N, 7°55'E; 1976–2016) [32]	Pretoria, South Africa (25°43'S, 28°21'E; 1973–1994) [21]
Jungfraujoch, Switzerland (46°33'N, 7°42'E; 1986–2019) [32–33]	Cape Grim, Australia (40°41'S, 144°41'E; 1994–2008) [36]
Izaña (28°22'N, 16°30'W; 1976–1990) and Mas Palomas (27°45'N, 15°40'W; 1973), Spain [1]	Wellington (41.25–41°S, 174.69–87°E; 1973–2019) [22] and
<i>Tree rings</i>	Campbell Is. (52.5°S, 169.2°E; 1973–1977) [20], New Zealand
Uppsala, Sweden (60°00'N, 17°38'E; 1980–1981) [5]	Palmer Station (64°46'27"S, 64°03'14"W; 2005–2007) [31], South
Schauinsland, Germany (48°N, 8°E; 1974–1985) [34]	Pole (89.98°S, 24.80°W; 1984–1992 [27] & 1999–2007 [31]) and
Niepolomice, Poland (50°02'N, 20°13'E; 1973–2003) [7]	Scott Base (77.9°S, 166.7°E; 1973–1976) [20], Antarctica
NE Hungary (47°35'N, 21°35'E; 1973–1978) [10]	<i>Tree rings</i>
NE Mexico (23°49'N, 99°50'W; 1973–2002) [13]	Muna Is., Indonesia (5°S, 122°E; 1973–1979) [19]
Shika-machi (37.1°N, 136.5°E; 1973–1999) [14] and Fukushima (37.01°N, 140.81°E; 1984–1989 & 1994) [35], Japan	Irruputuncu, Altiplano, Chile (20°S, 68°W; 1973–2014) [23]
Mts Chiak and Kyeryon, South Korea (37°20'–23'N, 128°03'–04'E; 1975–2000) [15]	Camanducaia, Brazil (22°50'S, 46°04'W; 1973–1997) [24]
Mandla, India (23°N, 81°E; 1980) [16]	Armidade (30°S, 152°E; 1973–1977) [25] and Tasmania (41°41'S, 145°18'E; 1973–1976) [17], Australia
Doi Inthanon, Thailand (18°33'N, 98°34'E; 1973–1975) [17]	Wellington (41.25–33°S, 174.87°E; 1973–2012) [22] and
	Campbell Is. (52.554°S, 169.133°E; 1973–2011) [26], New Zealand

Notes: [1] = Nydal and Lövsøth (1996); [2] = Levin and Kromer (2004); [3] = Berger et al. (1965) and Berger and Libby (1966, 1967, 1968, 1969); [4] = Svarva et al. (2019); [5] = Olsson and Possnert (1992); [6] = Kudsk et al. (2018); [7] = Rakowski et al. (2013); [8] = Stuiver et al. (1998); [9] = Grootes et al. (1989); [10] = Hertelendi and Csongor (1982); [11] = Cain et al. (2018); [12] = Damon et al. (1989); [13] = Beramendi-Orosco et al. (2018); [14] = Yamada et al. (2005); [15] = Park et al. (2002); [16] = Murphy et al. (1997); [17] = Hua et al. (2000); [18] = Hua et al. (2004); [19] = Hua et al. (2012); [20] = Manning et al. (1990); [21] = Vogel and Marais (1971); [22] = Turnbull et al. (2017); [23] = Ancapichún et al. (2021); [24] = Santos et al. (2015); [25] = Hua et al. (2003); [26] = Turney et al. (2018); [27] = Meijer et al. (2006); [28] = Graven et al. (2012a); [29] = Turnbull et al. (2007), Lehman et al. (2013), and Lehman and Miller (2019); [30] = Berger et al. (1987); [31] = Graven et al. (2012b); [32] = Levin and Kromer (2004), and Hammer and Levin (2017); [33] = Emmenegger et al. (2020); [34] = Levin and Kromer (1997); [35] = Xu et al. (2015); and [36] = Levin et al. (1996, 1999, 2011).

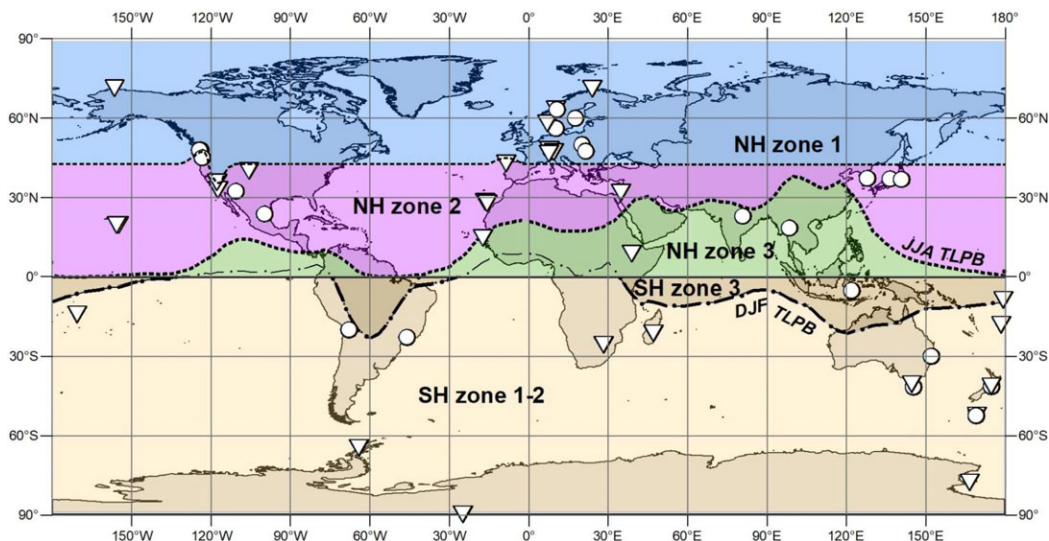


Figure 1 World map showing the zones and locations of atmospheric CO₂ sampling (triangles) for ¹⁴C analysis and Δ¹⁴C tree-ring records (circles) used for our compilation. The mean positions of the TLPB during December–February (DJF) and June–August (JJA) are based on the NCEP/NCAR sea level pressure data (Kalnay et al. 1996) for 1949–2019.

ZONAL ATMOSPHERIC Δ¹⁴C AND BOUNDARIES

As a result of aboveground nuclear detonations mostly in the NH, the majority of bomb ¹⁴C resided in the northern stratosphere during the years of intensive atmospheric nuclear testing and approximately one year after the 1963 Nuclear Test Ban Treaty (1962–1964) (Telegadas 1971; Hesshaimer and Levin 2000; Naegler and Levin 2006). Bomb ¹⁴C was injected into the troposphere through the mid- to high-latitude tropopause gaps during the springtime of each hemisphere. The seasonality of this exchange led to a ¹⁴C disequilibrium between the stratosphere and the troposphere during the early 1960s (Hesshaimer and Levin 2000), which was employed for constraining parameters related to atmospheric transport across the tropopause (Hesshaimer 1997; Levin et al. 2010). The excess-¹⁴C injection from the stratosphere also created large ¹⁴C gradients between tropospheric high and low latitudes, and between the northern and southern troposphere during ca. 1955–1967 (Hua and Barbetti 2007; Hua et al. 2012), which are valuable for modeling tropospheric air mass transport. Excess ¹⁴C was subsequently transferred southwards and the spatial distribution of tropospheric radiocarbon during this period is strongly influenced by atmospheric transport and mixing through the large-scale wind systems including monsoon circulation (Hua and Barbetti 2007; Levin et al. 2010; Hua et al. 2012). This spatial distribution seems to be further characterised by 5 zones of different Δ¹⁴C levels (NH zones 1, 2, and 3, and SH zones 3 and 1–2; see Figure 1) that decrease from north to south (Hua et al. 2013). NH zone 1 in northern mid- to high latitudes, where most of the excess ¹⁴C from the stratosphere was injected into the troposphere (e.g., Levin et al. 1985; Nydal and Gislefoss 1996), had the highest Δ¹⁴C values during this period. Meanwhile, at the same time, SH zone 1–2 covering most of the SH recorded the lowest Δ¹⁴C values, and the other zones recorded intermediate Δ¹⁴C levels. The intra-hemispheric differences in atmospheric Δ¹⁴C were substantially reduced in the late 1960s and early 1970s (Telegadas 1971; Manning

et al. 1990) as a result of atmospheric mixing, and from 1973 onwards there have been similar $\Delta^{14}\text{C}$ values between locations within each hemisphere (Hua et al. 2013). Similar to Hua et al. (2013), in this current study we employed the five-zone pattern of atmospheric $\Delta^{14}\text{C}$, which broadly reflects major zones of atmospheric circulation, with different zonal $\Delta^{14}\text{C}$ levels for 1950–1972 and very similar zonal $\Delta^{14}\text{C}$ values in each hemisphere for 1973–2019.

Figure 1 shows the zonal boundaries. The boundary between NH zone 2 and NH zone 3 is defined as the mean position of the convergence of northeasterly trade winds from the northern subtropics and winds from the northern and southern tropics during June, July and August (JJA). This convergence, known as the Inter-Tropical Convergence Zone (ITCZ), is associated with a low-pressure band (tropical low pressure belt (TLPB); Ancapichún et al. 2021). However, as the ITCZ is a marine phenomenon and is not well defined over the continents (e.g., Vuille et al 2012; Marsh et al. 2018), in this paper we use TLPB instead of ITCZ concerning the wind convergence associated with the low-pressure band. During December, January and February (DJF), the TLPB has a southward position, which is the convergence of winds from the northern tropics and easterly winds from the southern tropics and subtropics (Hogg et al. 2020; Ancapichún et al. 2021). The mean DJF position of the TLPB in the eastern Pacific, the eastern Atlantic and most of Central Africa is located in the NH. Therefore, for these regions SH zone 3 was not defined and the Equator was employed as the boundary between NH zone 3 and SH zone 1–2. The mean DJF position of the TLPB in the western Pacific, the Indian Ocean and South America is located in the SH and was used as the boundary between SH zone 3 and SH zone 1–2. It is worth noting that lower $\Delta^{14}\text{C}$ values over the Southern Ocean, related to air-sea gas exchange with ^{14}C -depleted surface ocean water that is generated by upwelling of intermediate and deeper ocean waters (ca. 3–6‰ during the late 1980s–the 2000s) compared to SH sub-tropical and temperate sites are well documented (Levin et al. 2010; Graven et al. 2012b; Turney et al. 2016) and there is some suggestion that it would be appropriate to define these areas as two separate zones. However, for the intended application of dating terrestrial materials, this applies only to a very limited subset of locations south of ca. 50°S. In addition, only a small amount of data is currently available for this region and highlights the need for further work over the Southern Ocean. Therefore, in the current compilation, results from SH zones 1 and 2 are binned into a single $\Delta^{14}\text{C}$ zone, SH zone 1–2.

The new tree-ring record from Irruputuncu, Altiplano, Chile at 20°S, 68°W (Ancapichún et al. 2021) is located close to the western edge of the South American “U-shaped” boundary between SH zone 3 and SH zone 1–2 derived from the NCEP/NCAR sea level pressure data (Kalnay et al. 1996) (Figure 1). Despite a minor portion of the air parcels (21%) reaching Irruputuncu from the Amazon basin (SH zone 3), its tree-ring $\Delta^{14}\text{C}$ values are similar to those from Wellington, New Zealand (Ancapichún et al. 2021) located in SH zone 1–2. Thus, appropriate development of new tree-ring records from low to mid-latitude regions is necessary as a means to better define the areas affected by changes in the mean TLPB position.

The boundary between NH zone 1 and NH zone 2 was previously defined based on limited ^{14}C records in mid- to high northern latitudes during the bomb peak period. According to Hua and Barbetti (2004) and Hua et al. (2013), this boundary around 40°N is located south of China Lake (CL; 35°32'N, 117°41'W) but north of Santiago de Compostela (42°53'N, 8°26'W). With the recent availability of the tree-ring record from western Oregon, USA (45°07'N, 123°27'W;

1960–1969; Cain et al. 2018) and the inclusion of a short tree-ring data set from Washington state, USA (47°57'N, 124°33'W; 1962–1964; Grootes et al. 1989), the position of this boundary in northwestern America can be refined.

Hua and Barbetti (2004) suggested that the CL atmospheric record (1963–1968) belonged to NH zone 1, based on the fact that the average of monthly $\Delta^{14}\text{C}$ differences between CL and NH zone 1 data, and between CL and NH zone 2 data are negligible and large, respectively. It is worth noting that higher $\Delta^{14}\text{C}$ values of the CL record compared to those of other atmospheric data sets at similar latitudes in NH zone 2 are not likely due to influences of nearby Nevada bomb tests on CL (see later discussion).

Figure 2 shows monthly $\Delta^{14}\text{C}$ differences between NH zone 1 and CL, and between NH zone 2 and CL. The CL $\Delta^{14}\text{C}$ values are similar to NH zone 1 values and higher than NH zone 2 values mostly during winter-spring (grey stripes in Figure 2), but lower than NH zone 1 values and similar to NH zone 2 values during summer-autumn (white stripes in Figure 2) except for late 1967–1968 due to reduced $\Delta^{14}\text{C}$ differences between regions in the late 1960s. These observations support large seasonal variations of the polar jet in north-western America as discussed in the literature (e.g., Barton and Ellis 2009; Pena-Ortiz et al. 2013). They also indicate that during the bomb peak period the polar jet moved southwards as far as south of CL in winter-spring and CL received air masses from the north containing higher $\Delta^{14}\text{C}$ values than southern air-masses, while in summer-autumn the polar jet travelled northwards resulting in a contribution of the southern air masses to CL.

In contrast, an oak tree from western Oregon, located northwest of CL, with radial growth during spring–late autumn has $\Delta^{14}\text{C}$ values close to those of NH zone 2 rather than NH zone 1 (Cain et al. 2018; Figure 3). The authors used the Pacific North American (PNA) index, representing a record of large-scale weather patterns that describe the placement of the polar and sub-tropical jets, to explain some relatively low values of their tree-ring $\Delta^{14}\text{C}$. They showed that monthly PNA index values for March–June were negative in 1962–1964, coinciding with relatively low tree-ring $\Delta^{14}\text{C}$ values during April–June of 1962–1964. This suggests during this period both the polar and sub-tropical jets moved northwards and their tree rings reflected carbon uptake from air masses coming from the south containing lower bomb $\Delta^{14}\text{C}$ values.

Furthermore, $\Delta^{14}\text{C}$ values of Sitka spruce tree rings from Washington state (Grootes et al. 1989) located north of the Oregon tree rings are similar to NH zone 1 values based on atmospheric records (Figure 3). Large seasonal variation in the position of the polar jet in north-western America discussed above means that the boundary between NH zone 1 and NH zone 2 varies seasonally. However, with the $\Delta^{14}\text{C}$ data during the bomb peak currently available for this region (CL atmospheric record, and Oregon and Washington tree-ring data) and for our practical purposes, the boundary between NH zone 1 and NH zone 2 is considered to be located between the two tree-ring sites and south of CL (see Figure 1). More tree-ring records in north-western America are useful for further refinement of the position of the boundary between NH zone 1 and NH zone 2 in this region.

One may argue that higher $\Delta^{14}\text{C}$ values of the CL record (1963–1968) compared to those of other atmospheric data sets at similar latitudes, belonging to NH zone 2, are due to influences of Nevada bomb tests on CL. There were quite a number of low-yield atmospheric nuclear bomb tests at Nevada (36.6–37.2°N, 115.9–116.4°W) during 1951–1958 and 1962 (UNSCEAR, 2000). In 1962, there were only 4 atmospheric nuclear weapon tests in July

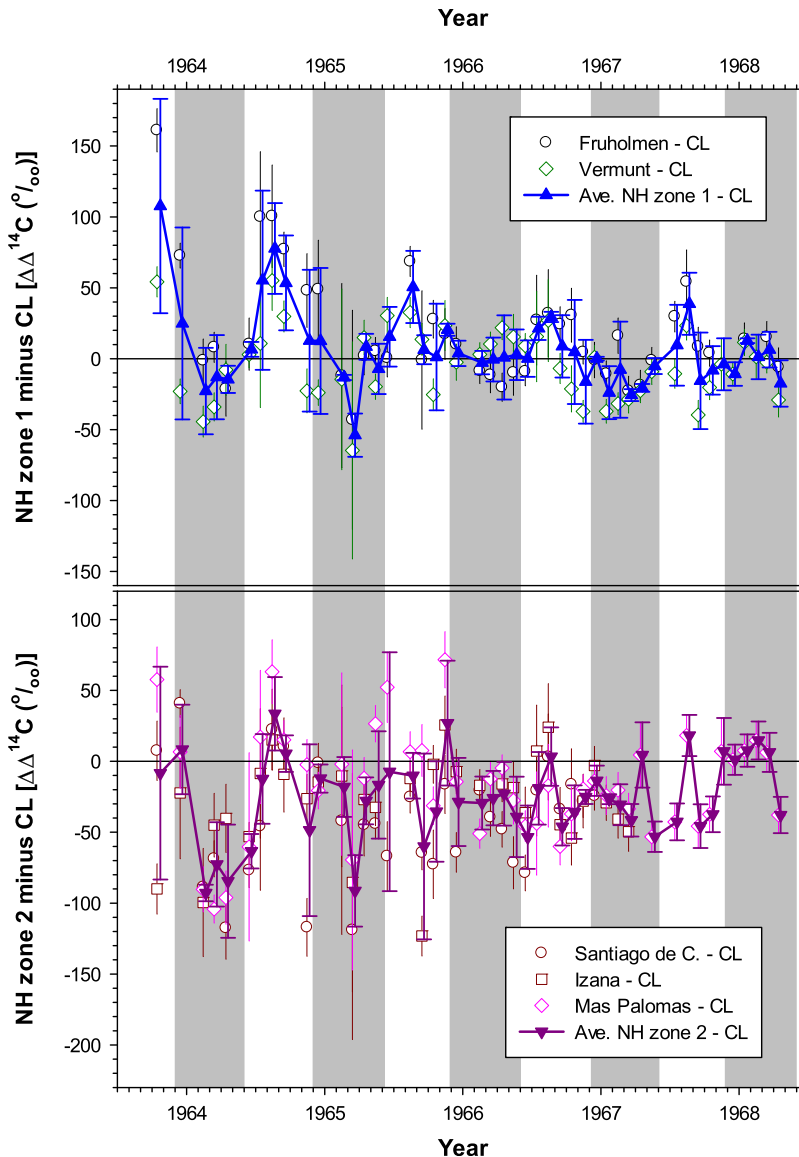


Figure 2 Monthly $\Delta^{14}\text{C}$ differences between atmospheric records in NH zones 1 and 2, and China Lake (CL). Data sources of these atmospheric records are Berger et al. (1965) and Berger and Libby (1966, 1967, 1968, 1969) for CL, Levin and Kromer (2004) for Vermunt, and Nydal and Lövseth (1996) for Fruholmen, Santiago de Compostela, Izaña and Mas Palomas. Grey and white stripes represent winter-spring and summer-autumn, respectively.

with a detonation yield ranging from 5 to 20 kton each. The Nevada test sites are located northeast of CL ($35^{\circ}32'\text{N}$, $117^{\circ}41'\text{W}$). Low-yield atmospheric nuclear bomb tests have a tendency to substantially contribute to local/regional areas (e.g., Enting 1982). If this were the case for these Nevada bomb tests in 1962, their contribution to CL would be clearly seen in 1962 and approximately one year after the tests (i.e., 1963). This is because

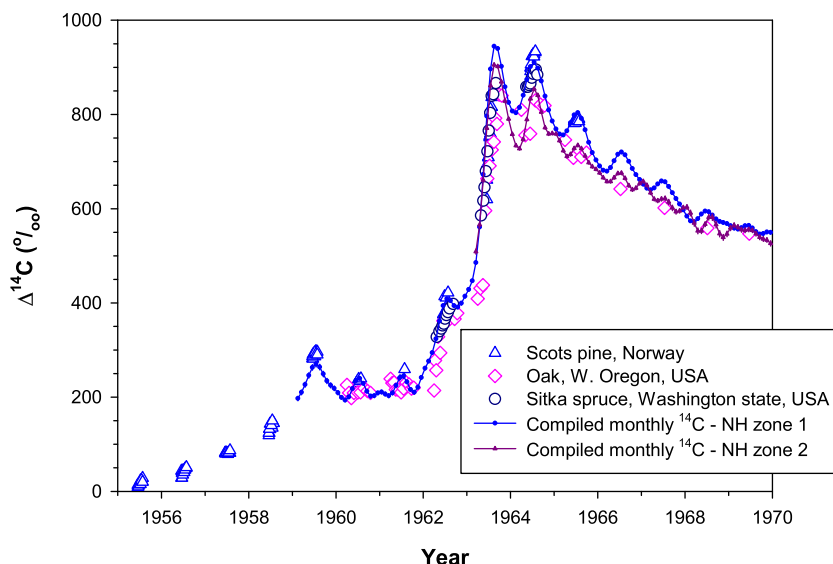


Figure 3 Tree-ring $\Delta^{14}\text{C}$ values from Scots pine (Norway; Svarva et al. 2019), oak (western Oregon, USA; Cain et al. 2018) and Sitka spruce (Washington state, USA; Grootes et al. 1989) versus compiled monthly $\Delta^{14}\text{C}$ data for NH zones 1 and 2 derived from atmospheric records (see discussions later on the construction of these compiled data).

atmospheric transport is quite fast, which is ca. 1 year from northern mid-latitudes to northern tropics based on the timing of the bomb $\Delta^{14}\text{C}$ peaks in atmospheric sampling (August 1963 in Vermont, Austria [Levin and Kromer 2004] and July 1964 in Dakar, Senegal [Nydal and Lövseth 1996]) for example. However, the two earliest CL $\Delta^{14}\text{C}$ values available in 1963 are similar to NH zone 2 values (Figure 2). In addition, CL $\Delta^{14}\text{C}$ values are higher than NH zone 2 values during winter-spring seasons in 1964–1965 (Figure 2), 2–3 years after the tests. These indicate that relatively high CL $\Delta^{14}\text{C}$ values during the bomb peak period are unlikely due to the contribution of the 1962 Nevada nuclear bomb tests.

COMPILATION METHODS

Timing of Tree-Ring Growth Seasons

Growth seasons of different tree-ring species in different regions employed in our compilation are not identical, but they are similar (e.g., Hua et al. 2012; Cain et al. 2018; Turney et al. 2018; Svarva et al. 2019; Ancapichún et al. 2021). The duration of growing seasons can also vary slightly from one year to another. However, tree growth follows a similar pattern of slow increment at the start (early spring to early summer) and end (late summer to autumn) of a growing season, while fast increment occurs during summer (Grootes et al. 1989; Hua et al. 2000; Turnbull et al. 2017; Cain et al. 2018; Kudsk et al. 2018; Svarva et al. 2019). This also applies to tropical tree rings used in the current compilation for which most growth occurs in summer rainy seasons (e.g., Hua et al. 2000, 2012). In addition, for each annual ring, wood material away from the ring boundaries is usually sampled for ^{14}C analysis (e.g., Hua et al. 1999, 2012) to avoid potential cross-ring-boundary issues. Thus, the material of each ring selected for ^{14}C analysis is mainly the portion of wood growing in summer in both hemispheres (May–August or the middle of the current year for the NH,

and November–February or the beginning of the following year for the SH). This simple approach allows for estimation of hemispheric and global summer means from tree-ring $\Delta^{14}\text{C}$ values and associated atmospheric $\Delta^{14}\text{C}$ values in addition to the construction of the zonal estimates.

Compiled Data

Our compilation provides both summer and monthly results. The summer data were derived from atmospheric sampling and tree-ring records using a simple averaging method. Monthly data were primarily based on atmospheric sampling, with tree-ring data only used when atmospheric CO_2 data were not available, mostly during the pre-bomb and early bomb period. A curve fitting method was employed to construct monthly results.

Summer Data

Zonal, hemispheric, and global summer data sets were compiled. Five separate zonal data sets (3 for the NH and 2 for the SH) were constructed for the period 1950–1972. Due to similar $\Delta^{14}\text{C}$ values between locations in each hemisphere from 1973 onwards (Hua et al. 2013), 3 identical zonal data sets for the NH and 2 identical zonal data sets for the SH were compiled. We modified the methods employed by Hua et al. (2013) for the construction of these summer data sets, which are described below.

The mean value for summers (May–August for the NH (Hua and Barbetti 2004; Hammer and Levin 2017) and November–February for the SH (Hua and Barbetti 2004)) for an atmospheric $\Delta^{14}\text{C}$ record for a particular year was calculated only if there were data available for at least 3 out of 4 months for the season. The mean summer value for a particular zone in a particular year was then calculated with weight being the uncertainty associated with the summer mean of the individual record (atmospheric sampling or tree rings).

As the surface areas covered by the three NH zones are different in size (Figure 1), summer mean values for the NH for the period 1950–1972 were calculated from the 3 zonal summer means, with weights being the percentages of zonal surface areas (ca. 17%, 46%, and 37% for NH zones 1, 2, and 3, respectively). The same approach was employed for the calculation of summer mean values for the SH for 1950–1972 with the percentages of zonal surface areas for SH zones 3 and 1–2 being ca. 15% and 85%, respectively. For the period 1973–2019, hemispheric summer mean values are actual zonal summer values.

Two zonal (SH zones 3 and 1–2) data sets for boreal summers were also compiled to construct the global boreal summer data set. For 1950–1972, the global boreal summer means were calculated using the 5 zonal (boreal summer) data sets with weights being the percentages of zonal surface areas mentioned above. For the period 1973–2019, the global boreal summer means were calculated using the 2 hemispheric data sets for boreal summers.

Monthly Data

Five zonal monthly data sets were constructed using the cgcrrv curve fitting method (Thoning et al. 1989) to output smooth curves at monthly resolution. The data used for the curve fitting were primarily atmospheric records. When atmospheric records were not available (e.g., mostly the pre-bomb and early bomb period), average zonal summer data and/or sub-annual tree-ring data were employed. In addition, to avoid possible discontinuities between our NH monthly data sets and IntCal20 curve (Reimer et al. 2020) when they are used together for dating, we included the raw IntCal20 data for 1941–1950 in our curve fitting. The same approach was

applied for the construction of the SH monthly data sets by including the raw SHCal20 data for 1941–1950 (Hogg et al. 2020).

To develop the smooth curves, all data for a given zonal data set were compiled, then a smooth curve was created following the method of Turnbull et al. (2017). Each data set was split into six time intervals (1941–1955, 1954–1966, 1965–1973, 1972–1990, 1989–2006, and 2005–2020) to allow the seasonal cycle and long-term trend to vary through time. The parameters used in the ccgrv curve fitting are interval = 365, cutoff1=180 and cutoff2 = 1900 for the early periods when only tree-ring data were available, and interval = 14, cutoff1=180 and cutoff2 = 667 for the other periods. A Monte Carlo method with 1000 iterations was used to create a smooth curve for each time interval, with uncertainty assigned from the scatter of the Monte Carlo simulation. For each of the 1000 simulations, the ^{14}C value for each date sampled is re-assigned randomly according to the normal distribution described by the mean and reported standard deviation of the measurement. A curve is fitted to each of the 1000 simulations, then the mean and standard deviation are calculated for each time step from the spread of the 1000 fitted curves. In this simulation, input data was at its native resolution (i.e., every raw data point was included), and the fitted curves were output at monthly resolution.

Finally, all six time intervals were spliced together, averaging across the overlap periods, to produce a smooth curve fit for the entire period. Alternative curve fitting methods do allow varying seasonal cycles (e.g., Pickers and Manning 2015), but require gap filling with interpolated data, which introduces a different set of biases.

For the pre-bomb and early bomb period and a short period 1970–1972 in NH zone 3 when only tree-ring data were available (except for SH zone 1–2 where atmospheric data were available), it is not possible to derive a seasonal cycle from the (summertime only) tree-ring data. It is also inappropriate to assign the seasonal cycle for the latter time period, as it is clear that the $\Delta^{14}\text{C}$ seasonal cycle changed dramatically with the inputs of bomb ^{14}C . Therefore, we chose not to assign any seasonal cycle to these periods, instead of interpolating the interannual trend to provide monthly $\Delta^{14}\text{C}$ values.

RESULTS AND DISCUSSION

Many plants and some animals depend on the carbon formed during the summer growing season, making the compiled zonal summer data sets appropriate for use in radiocarbon dating of these sample types. However, for other plants and vegetation, whose main growing seasons are different such as early-spring for leaves, autumn plants/seeds and winter wheat/rice, the zonal summer data sets are not useful for dating of these materials. Vegetation in the aseasonal tropics between $\sim 5^\circ\text{N}$ and $\sim 5^\circ\text{S}$, growing almost all year round, is also in this category. In addition, humans and animals, who consume foods mostly imported from around the globe, may not be accurately dated using the zonal summer data sets. We, therefore, take a simple and consistent approach, and recommend the compiled zonal monthly data sets should be used for dating of all recent samples.

Similar to the previous compilations (Tans 1981; Hua and Barbetti 2004; Hua et al. 2013; Graven et al. 2017), we aimed to provide compiled $\Delta^{14}\text{C}$ data sets with annual resolution for use in carbon cycle modeling. Summer data sets were chosen as their raw data were the only data available for the whole period of interest, 1950–2019. In addition, an advantage of these summer data sets is that they can be extended back in time using compatible

tree-ring based IntCal20 or SHCal20 data, if longer data sets are required for modeling studies. The zonal monthly data sets were constructed for dating purposes as discussed above. However, they can be used for carbon cycle modeling if it requires higher temporal resolution.

Compiled zonal atmospheric $\Delta^{14}\text{C}$ data sets for NH zones 1, 2, and 3 for boreal summers (May–August) for the period 1950–2019 are presented in Supplementary Table S1a, while compiled zonal atmospheric $\Delta^{14}\text{C}$ data sets for SH zones 3 and 1–2 for austral summers (November–February) are reported in Supplementary Table S1b. All the compiled zonal $\Delta^{14}\text{C}$ data sets are illustrated in Figure 4a. Compiled hemispheric $\Delta^{14}\text{C}$ data sets for boreal and austral summers are also reported in Supplementary Table S1a and Table S1b, respectively, while the compiled global atmospheric $\Delta^{14}\text{C}$ data set for boreal summers is presented in Supplementary Table S1c. The compiled hemispheric and global atmospheric $\Delta^{14}\text{C}$ data sets for 1950–2019 are also depicted in Figure 4b.

Our compiled summer $\Delta^{14}\text{C}$ data sets have good agreement with those of Hua et al. (2013) for the overlapping periods (1950–2010 for the NH and 1950–2011 for the SH; see Supplementary Figures S1a–h). The compilation by Graven et al. (2017) for 1950–2015 consists of annual $\Delta^{14}\text{C}$ data for 3 different regions, NH north of 30°N (NH> 30°N), 30°N – 30°S and SH south of 30°S (SH> 30°S), with the timing of each data point being in the middle of a year. For ease of comparison with our compiled data for the SH with each data point being the beginning of the following year, the compiled data for 2 regions 30°N – 30°S and SH> 30°S from Graven et al. (2017) were linearly interpolated (see Supplementary Figures S2c–d). In general, we find good concordance between our and their compiled $\Delta^{14}\text{C}$ data (Supplementary Figures S2a–d), although the spatial coverage of the study regions in these two studies are not the same.

Compiled zonal data sets at monthly resolution for 1941–2019, in $\Delta^{14}\text{C}$ and F^{14}C (Reimer et al. 2004), are reported in Supplementary Tables S2a–e. These data in F^{14}C are also shown in Figure 5. The ccgcrv curve fitting method used for the compilation of monthly data sets in this study has a couple of advantages compared to the weighted average methods used by Hua et al. (2013). First, the curve fitting method smooths the noise associated with the relatively large uncertainties assigned to individual measurements, resulting in smoother compiled data with clear seasonal cycles for the periods covered by atmospheric $\Delta^{14}\text{C}$ records (Figures 5 and 6a–e). Second, the compiled extended monthly data sets of Hua et al. (2013) have different temporal resolutions with monthly data for the periods covered by atmospheric $\Delta^{14}\text{C}$ records and annual summer data outside these periods. Meanwhile, the compiled data sets in the current study have a monthly resolution for the whole period of 1941–2019 (see Figures 6a–e; Supplementary Tables S2a–e). Thus, the curve fitting method used in the present study resulted in improved zonal monthly data sets and consequently improved radiocarbon dating of recent terrestrial samples.

Good agreement between the compiled monthly data sets and IntCal20 or SHCal20 is observed for the overlapping period (1941–1950) (Supplementary Figures S3a–e), indicating the continuity between these data sets when they are used together for radiocarbon dating. We recommend that when calibrations span the pre- and post-bomb periods, users replace the IntCal20 or SHCal20 data for 1941–1950 with the compiled monthly data for 1941–1950 to avoid discontinuities between the datasets.

The compiled monthly data sets for the NH zones in this study agree well with those of Hua et al. (2013) for the overlapping period (1950–2009) (Figures 6a–c). It should be noted that the

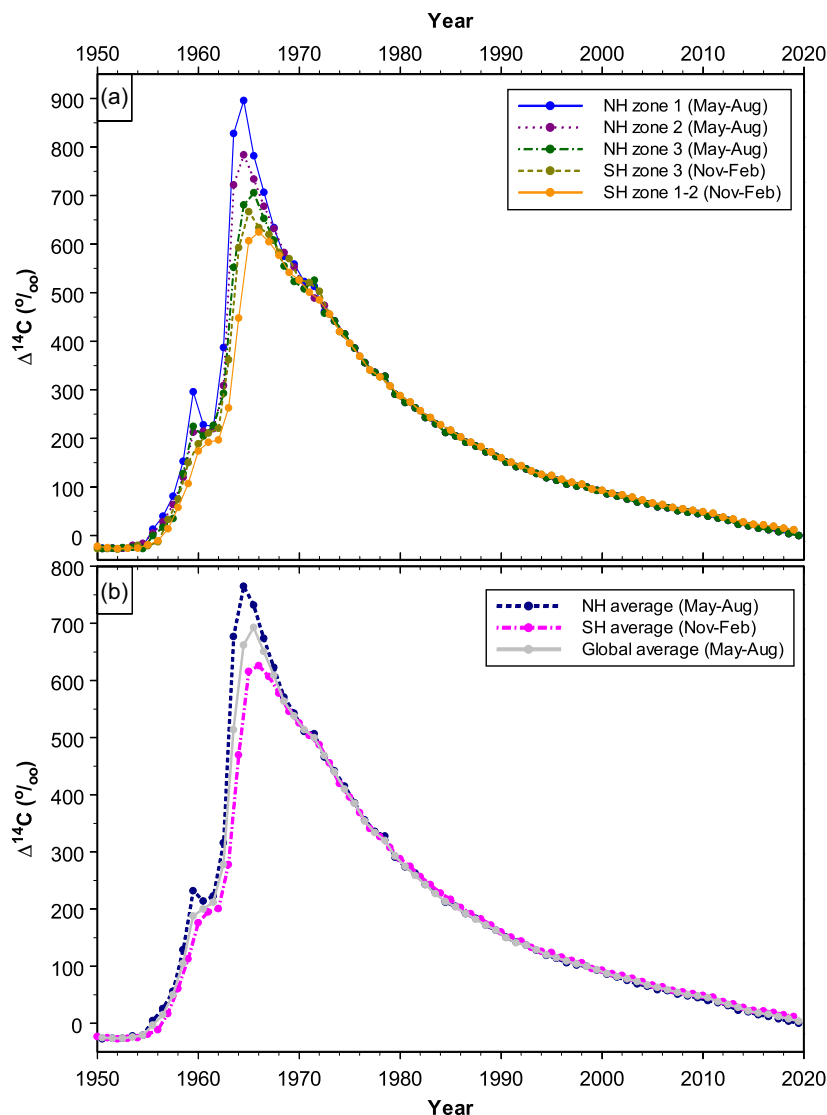


Figure 4 Compiled zonal (a), and hemispheric and global (b) summer atmospheric $\Delta^{14}\text{C}$ curves. The compiled data sets are reported in Supplementary Tables S1a–c.

Monte Carlo simulation associated with the curve fitting method assigns smaller uncertainties than the standard deviations that were assigned in the previous study.

For the SH zones, a similar pattern is observed except during 1990–1993 (Figures 6d–e). With the revision of the Wellington atmospheric $\Delta^{14}\text{C}$ record for 1990–1993 (Turnbull et al. 2017), our compiled monthly F^{14}C data for the SH zones for this period are lower than those of the 2013 data (Figures 6d–e). This means anomalously high F^{14}C values for this period, which previously appeared in the 2013 data for the SH zones, no longer exist in our compiled monthly data. Similarly, anomalously high $\Delta^{14}\text{C}$ values for 1990–1993, previously

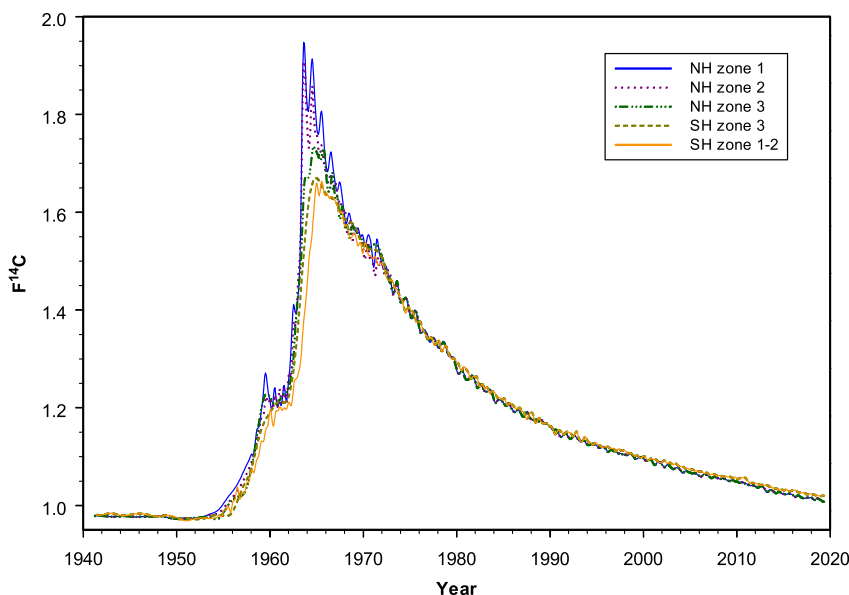


Figure 5 Compiled monthly atmospheric $F^{14}\text{C}$ curves for 5 different zones. The compiled data sets are presented in Supplementary Tables S2a–e.

appearing in the compiled summer data of Hua et al. (2013) for the SH zones, are also not evident in our compiled summer data (see Supplementary Figures S1d–e).

The compiled monthly $F^{14}\text{C}$ data are mostly based on atmospheric records, but they are derived from tree-ring records when atmospheric sampling is not available (Figures 6a–e). The use of tree-ring data to extend the compiled monthly atmospheric-based data is an advantage. However, tree rings do not fully represent atmospheric $\Delta^{14}\text{C}$ levels when these levels change substantially and quickly, although tree-ring $\Delta^{14}\text{C}$ follows atmospheric $\Delta^{14}\text{C}$ very well with a delay of no more than ca. 2 weeks for Washington Sitka spruce (Grootes et al. 1989) or 5–6 weeks for Tasmanian Huon pine (Hua et al. 2000). For example, atmospheric $F^{14}\text{C}$ (and consequently $\Delta^{14}\text{C}$) in NH zone 1 peaks in 1963 (Figure 5) but tree-ring $\Delta^{14}\text{C}$ in this zone reaches its maximum in 1964 (Figure 4a). Another example, which can be seen in Figure 3, indicates that sub-annual tree-ring $\Delta^{14}\text{C}$ for the NH zones 1 and 2 during 1963–1964 do not cover the full ranges of their associated atmospheric $\Delta^{14}\text{C}$ values. These differences are likely due to growing seasons, which are only a portion of a year, seasonal averaging or insufficient sampling resolution for tree rings. Substantial changes in atmospheric $\Delta^{14}\text{C}$ levels occur during the early bomb period and the bomb peak period. During these periods, needles/leaves of early spring, autumn plants/seeds and winter wheat/rice incorporate atmospheric $\Delta^{14}\text{C}$ values at the time of growth, which may be substantially different from those of annual and/or sub-annual tree rings. This issue, therefore, should be considered or recognized when dating such samples for the periods that the compiled monthly ^{14}C data are derived from tree-ring records such as 1955–1959 for NH zone 1, 1955–1963 for NH zones 2 and 3, and especially 1955–1972 for SH zone 3 (see Figures 6a–d).

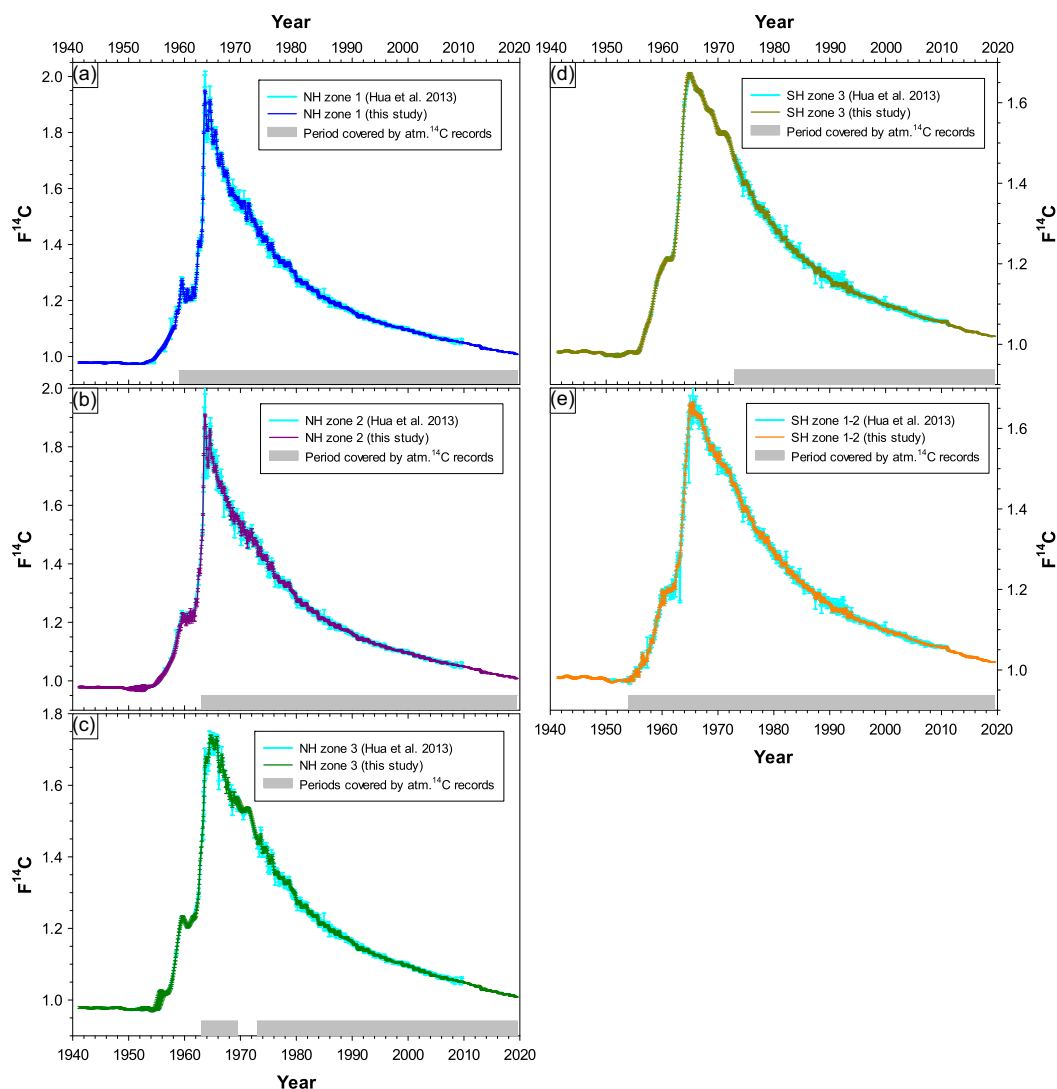


Figure 6 Our compiled monthly atmospheric $F^{14}C$ curves versus those of Hua et al. (2013).

After reaching its peak levels, atmospheric $\Delta^{14}C$ in the NH and SH has decreased since 1963–1964 and 1964–1965, respectively. Decreases in atmospheric $\Delta^{14}C$ from the mid-1960s to mid-1980s are mainly due to rapid exchange between the atmosphere and the biosphere and oceans (Oeschger et al. 1975; Druffel and Suess 1983; Levin and Heshaimer 2000), while combustion of fossil fuels free of ^{14}C is the main causal factor for the $\Delta^{14}C$ decline since the late 1980s and early 1990s (Levin et al. 2010; Graven et al. 2012a). Since the early and late 2000s, the atmospheric $\Delta^{14}C$ values have been lower than those of the surface waters in the North and South Pacific Gyres, respectively, indicating the oceans might become a net ^{14}C source (instead of a net ^{14}C sink) of the atmosphere (Andrews et al. 2016, 2021; Wu et al. 2021).

The last data points in our compiled monthly data at 2019.375 have respective $F^{14}\text{C}$ values of 1.0084 and 1.0195 for the NH and SH (see Supplementary Tables 2a–e), which are very close to the pre-bomb $F^{14}\text{C}$ value of slightly lower than 1. This indicates that clean-air $F^{14}\text{C}$ is likely to reach the pre-bomb value in the early 2020s, which is similar to the estimation of Graven (2015) and Sierra (2018). If this occurs, radiocarbon dating of a single terrestrial sample having $F^{14}\text{C}$ lower than 1 delivers two possible ages: pre-1955 and the early 2020s or after. Graven (2015) discussed issues of radiocarbon dating of single samples with different scenarios of fossil-fuel emissions, suggesting that the radiocarbon method may not provide definitive ages for samples up to 2000 years old under a worst-case, high-emission scenario from fossil fuels. To avoid these issues, radiocarbon dating of a series of samples in sequence with known chronological ordering (e.g., samples from a sediment profile or along the growth axis of a tree) combined with other isotopic studies should be employed. Constraints in the chronological ordering of measured radiocarbon ages (or $F^{14}\text{C}$ values) of the sequence samples give a much better indication (than that of a single sample) on their calendar ages, resulting in more definite ages for each sample in the sequence (e.g., Goslar et al. 2005; Yeloff et al. 2006; Hua 2009; Santini et al. 2013). As fossil fuels are not only depleted in ^{14}C ($F^{14}\text{C} = 0$ and $\Delta^{14}\text{C} = -1000\text{‰}$) but also in ^{13}C ($\delta^{13}\text{C} = -28\text{‰}$, which is $\sim 20\text{‰}$ lighter than atmospheric $\delta^{13}\text{C}$), the decline of $\delta^{13}\text{C}$ due to fossil fuel input can be useful to distinguish between the two possible ages (Köhler 2016). For example, if measured $\delta^{13}\text{C}$ values of dated C3 and C4 plant samples are lower than their present-day ranges of -34 to -22‰ (Diefendorf et al. 2010; Kohn 2010; Basu et al. 2015) and -16 to -10‰ (Cerling and Harris 1999; Basu et al. 2015), respectively, it is likely that these samples are formed or grown in this decade or after.

CONCLUSION AND FUTURE RESEARCH

A comprehensive compilation of clean-air $\Delta^{14}\text{C}$ for the period 1950–2019 is presented. The compilation consists of zonal, hemispheric, and global summer $\Delta^{14}\text{C}$ data sets for use in regional and global carbon cycle studies. Compiled monthly $F^{14}\text{C}$ (and $\Delta^{14}\text{C}$) data sets for 5 different zones (3 in the NH and 2 in the SH) are also reported. These monthly data sets are used as zonal radiocarbon calibration curves in the CALIBomb (<http://calib.org/CALIBomb/>) and OxCal (<http://c14.arch.ox.ac.uk/calibration.html>) programs for age calibration of dated terrestrial samples formed after 1955.

Atmospheric and tree-ring $\Delta^{14}\text{C}$ records selected for our compilation are not distributed evenly around the globe (Figure 1). The majority of the records are from Europe, northwestern America and East Asia for the NH, and New Zealand, southeastern Australia and Antarctica for the SH. Future research efforts should focus first on new sites for better determination of zonal boundaries for improved bomb radiocarbon dating. They include southern Europe, northeastern America, northern China and southern Russia for NH zone 1–NH zone 2 boundary; central America, north-central Africa and northern China for NH zone 2–NH zone 3 boundary; and south America, south-central Africa and northern Australia for SH zone 3–SH zone 1–2 boundary. Tree rings during the bomb peak period from these new sites are useful for the determination of zonal boundaries. The quality of tree-ring $\Delta^{14}\text{C}$ data should also be considered by applying the dendrochronological methods for tree-ring dating instead of ring counting, specifying how wood material is

sampled and employing sufficient sample pretreatment to extract holocellulose or alpha-cellulose for ^{14}C analysis.

For periods not covered by atmospheric records (the early bomb period for NH zones 1, 2, and 3, and 1955–1972 for SH zone 3; see Figures 6a–d), the compiled monthly F^{14}C data sets are currently based on tree rings. Therefore, for these periods, $\Delta^{14}\text{C}$ data from archived seasonal plants, seeds, wheat, rice, etc., whose growth seasons are different than summer (the main growing season of tree rings), should be useful for the improvement of the compiled zonal monthly data sets.

Finally, some records used here are relatively short, or need to be replicated and/or possibly revised. Data were produced before methodological and instrumentation updates, without clear data-quality information or data replication (see details in references therein Table 1). With the purpose of data enhancement and enrichment, follow-up studies on existing sites should be encouraged to corroborate atmospheric ^{14}C records, following the criteria layout here. Future compilations would require further screening of data sets and aggregation of new records.

ACKNOWLEDGMENTS

We thank S. Hankin for the preparation of Figure 1, H. Erlenkeuser for the pretreatment of Kiel tree rings, S. Xu for the dating of Fukushima tree rings, and H. Svarva, M.-J. Nadeau, and P. Grootes for their generous provision of unpublished $\Delta^{14}\text{C}$ data on sub-annual Washington Sitka spruce measured at the National Laboratory for Age Determination in Trondheim. We would also like to thank P. Grootes for useful discussions and comments on age calibration using compiled monthly $\Delta^{14}\text{C}$ data derived from tree rings. We also acknowledge two anonymous reviewers and the Associate Editor, P. Reimer, for their valuable comments, which improved the manuscript.

SUPPLEMENTARY MATERIAL

To view supplementary material for this article, please visit <https://doi.org/10.1017/RDC.2021.95>

REFERENCES

- Ancapichún S, De Pol-Holz R, Christie DA, Santos GM, Collado-Fabbri S, Garreaud R, Lambert F, Orfanioz-Chequela A, Rojas M, Southon J, Turnbull JC, Creasman PP. 2021. Radiocarbon bomb-peak signal in tree-rings from the tropical Andes register low latitude atmospheric dynamics in the Southern Hemisphere. *Science of the Total Environment* 774:145126. doi: [10.1016/j.scitotenv.2021.145126](https://doi.org/10.1016/j.scitotenv.2021.145126).
- Andrews AH, Siciliano D, Potts DC, DeMartini EE, Covarrubias S. 2016. Bomb radiocarbon and the Hawaiian Archipelago: coral, otoliths and seawater. *Radiocarbon* 58:531–548.
- Andrews AH, Prouty NG, Cheriton OM. 2021. Bomb-produced radiocarbon across the South Pacific Gyre – a new record from American Samoa with utility for fisheries science. *Radiocarbon*. doi: [10.1017/RDC.2021.51](https://doi.org/10.1017/RDC.2021.51)
- Barton NP, Ellis AW. 2009. Variability in wintertime position and strength of the North Pacific jet stream as represented by re-analysis data. *International Journal of Climatology* 29:851–862. doi: [10.1002/joc.1750](https://doi.org/10.1002/joc.1750).
- Basu S, Agrawal S, Sanyal P, Mahato P, Kumar S, Sarkar A. 2015. Carbon isotopic ratios of modern C_3 – C_4 plants from the Gangetic Plain, India and its implications to paleovegetational reconstruction. *Palaeogeography, Palaeoclimatology, Palaeoecology* 440: 22–32.
- Berger R, Fergusson GJ, Libby WF. 1965. UCLA radiocarbon dates IV. *Radiocarbon* 7: 336–371.

- Berger R, Jackson TB, Michael R, Suess HE. 1987. Radiocarbon content of tropospheric CO_2 at China Lake, California 1977–1983. *Radiocarbon* 29(1):18–23.
- Berger R, Libby WF. 1966. UCLA radiocarbon dates V. *Radiocarbon* 8:467–497.
- Berger R, Libby WF. 1967. UCLA radiocarbon dates VI. *Radiocarbon* 9:477–504.
- Berger R, Libby WF. 1968. UCLA radiocarbon dates VIII. *Radiocarbon* 10(2):402–416.
- Berger R, Libby WF. 1969. UCLA radiocarbon dates IX. *Radiocarbon* 11(1):194–209.
- Beramendi-Orosco LE, Johnson KR, Noronha AL, González-Hernández G, Villanueva-Díaz J. 2018. High precision radiocarbon concentrations in tree rings from Northeastern Mexico: a new record with annual resolution for dating the recent past. *Quaternary Geochronology* 48:1–6. doi: [10.1016/j.quageo.2018.07.007](https://doi.org/10.1016/j.quageo.2018.07.007).
- Cain WF, Griffin S, Druffel-Rodriguez KC, Druffel ERM. 2018. Uptake of carbon for cellulose production in a white oak from Western Oregon, USA. *Radiocarbon* 60(1):151–158. doi: [10.1017/RDC.2017.82](https://doi.org/10.1017/RDC.2017.82).
- Carbone M, Czimczik C, Keenan T, Murakami P, Pederson N, Schaberg P, Xu X, Richardson A. 2013. Age, allocation and availability of nonstructural carbon in mature red maple trees. *New Phytologist* 200:1145–1155. doi: [10.1111/nph.12448](https://doi.org/10.1111/nph.12448).
- Cerling TE, Harris JM. 1999. Carbon isotope fractionation between diet and bioapatite in ungulate mammals and implications for ecological and paleoecological studies. *Oecologia* 120:347–363.
- Damon PE, Cheng S, Linick TW. 1989. Fine and hyperfine structure in the spectrum of secular variations of atmospheric ^{14}C . *Radiocarbon* 31(3):704–718.
- Diefendorf AF, Mueller KE, Wing SL, Koch PL, Freeman KH. 2010. Global patterns in leaf ^{13}C discrimination and implications for studies of past and future climate. *Proceedings of the National Academy of Sciences* 107:5738–5743.
- Druffel EM, Suess HE. 1983. On the radiocarbon record in banded corals: exchange parameters and net transport of $^{14}\text{CO}_2$ between atmosphere and surface ocean. *Journal of Geophysical Research* 88(C2):1271–1280.
- Emmenegger L, Leuenberger M, Steinbacher M., ICOS RI. 2020. ICOS ATC 14C release, Jungfraujoch (10.0 m), 2016-01-04–2019-08-12. <https://hdl.handle.net/11676/X-XPkZIO4DWX7wnCsLQ7akY>.
- Enting IG. 1982. Nuclear weapons data for use in carbon cycle modeling. CSIRO Division of Atmospheric Physics Technical Paper No. 44. Melbourne: CSIRO.
- Goodsite ME, Rom W, Heinemeier J, Lange T, Ooi S, Appleby PG, Shotyk W, van der Knaap WO, Lohse C, Hansen TS. 2001. High-resolution AMS ^{14}C dating of post-bomb peat archives of atmospheric pollutants. *Radiocarbon* 43(2B):495–515.
- Goslar T, van der Knaap WO, Hicks S., Andrič M, Czernik J, Goslar E, Räsänen S, Hyötylä, H., 2005. Radiocarbon dating of modern peat profiles: pre and post-bomb ^{14}C variations in the construction of age-depth models. *Radiocarbon* 47:115–134.
- Graven H, Allison CE, Etheridge DM, Hammer S, Keeling RF, Levin I, Meijer HAJ, Rubino M, Tans PP, Trudinger CM, Vaughn BH, White JWC. 2017. Compiled records of carbon isotopes in atmospheric CO_2 for historical simulations in CMIP6. *Geoscientific Model Development* 10:4405–4417. doi: [10.5194/gmd-10-4405-2017](https://doi.org/10.5194/gmd-10-4405-2017).
- Graven HD. 2015. Impact of fossil fuel emissions on atmospheric radiocarbon and various applications of radiocarbon over this century. *Proceedings of National Academy of Sciences USA* 112:9542–9545. doi: [10.1073/pnas.1504467112](https://doi.org/10.1073/pnas.1504467112).
- Graven HD, Guilderson TP, Keeling RF. 2012a. Observations of radiocarbon in CO_2 at La Jolla, California, USA 1992–2007: analysis of the long-term trend. *Journal of Geophysical Research* 117:D02302. doi: [10.1029/2011JD016533](https://doi.org/10.1029/2011JD016533).
- Graven HD, Guilderson TP, Keeling RF. 2012b. Observations of radiocarbon in CO_2 at seven global sampling sites in the Scripps flask network: analysis of spatial gradients and seasonal cycles. *Journal of Geophysical Research* 117:D02303. doi: [10.1029/2011JD016535](https://doi.org/10.1029/2011JD016535).
- Grootes PM, Farwell GW, Schmidt FH, Leach DD, Stuiver M. 1989. Rapid response of tree cellulose radiocarbon content to changes in atmospheric $^{14}\text{CO}_2$ concentration. *Tellus* 41B:134–148.
- Hammer S, Levin I. 2017. Monthly mean atmospheric $\Delta^{14}\text{CO}_2$ at Jungfraujoch and Schauinsland from 1986 to 2016. doi: [10.11588/data/10100](https://doi.org/10.11588/data/10100).
- Hertelendi E, Csongor E. 1982. Anthropogenic ^{14}C excess in the troposphere between 1951 and 1978 measured in tree rings. *Radiochemical and Radioanalytical Letters* 56:103–110.
- Hesshaimer V. 1997. Tracing the global carbon cycle with bomb radiocarbon [PhD thesis]. Heidelberg, Germany: University of Heidelberg.
- Hesshaimer V, Levin I. 2000. Revision of the stratospheric bomb $^{14}\text{CO}_2$ inventory. *Journal of Geophysical Research* 105:11,641–11,658.
- Hogg A, Heaton TJ, Hua Q, Palmer JG, Turney CSM, Southon J, Bayliss A, Blackwell PG, Boswijk G, Bronk Ramsey C, Pearson C, Petchey F, Reimer P, Reimer R, Wacker L. 2020. SHCal20 Southern Hemisphere calibration, 0–55,000 years cal BP. *Radiocarbon* 62(4):759–778. doi: [10.1017/RDC.2020.59](https://doi.org/10.1017/RDC.2020.59).

- Hua Q. 2009. Radiocarbon: a chronological tool for the recent past. *Quaternary Geochronology* 4: 378–390. doi: [10.1016/j.quageo.2009.03.006](https://doi.org/10.1016/j.quageo.2009.03.006).
- Hua Q, Barbetti M. 2004. Review of tropospheric bomb radiocarbon data for carbon cycle modeling and age calibration purposes. *Radiocarbon* 46(3):1273–1298.
- Hua Q, Barbetti M. 2007. Influence of atmospheric circulation on regional $^{14}\text{CO}_2$ differences. *Journal of Geophysical Research* 112: D19102. doi: [10.1029/2006JD007898](https://doi.org/10.1029/2006JD007898).
- Hua Q, Barbetti M, Jacobsen GE, Zoppi U, Lawson EM. 2000. Bomb radiocarbon in annual tree rings from Thailand and Tasmania. *Nuclear Instruments and Methods in Physics Research B* 172(1–4):359–365.
- Hua Q, Barbetti M, Levchenko VA, D'Arrigo RD, Buckley BM, Smith AM. 2012. Monsoonal influences on Southern Hemisphere $^{14}\text{CO}_2$. *Geophysical Research Letters* 39: L19806. doi: [10.1029/2012GL052971](https://doi.org/10.1029/2012GL052971).
- Hua Q, Barbetti M, Worbes M, Head J, Levchenko VA. 1999. Review of radiocarbon data from atmospheric and tree ring samples for the period 1945–1997 AD. *IAWA Journal* 20:261–283.
- Hua Q, Barbetti M, Zoppi U. 2004. Radiocarbon in annual tree rings from Thailand during the pre-bomb period, AD 1938–1954. *Radiocarbon* 46(2):925–932.
- Hua Q, Barbetti M, Zoppi U, Chapman DM, Thomson B. 2003. Bomb radiocarbon in tree rings from northern New South Wales, Australia: implications for dendrochronology, atmospheric transport and air-sea exchange of CO_2 . *Radiocarbon* 45(3):431–447.
- Hua Q, Barbetti M, Rakowski AZ. 2013. Atmospheric radiocarbon for the period 1950–2010. *Radiocarbon* 55:2059–2072. doi: [10.2458/azu_js_rc.v55i2.16177](https://doi.org/10.2458/azu_js_rc.v55i2.16177).
- Kalnay E, Kanamitsu M, Kistler R, Collins W, Deaven D, Gandin L, Iredell M, Saha S, White G, Woollen J, Zhu Y, Chelliah M, Ebisuzaki W, Higgins W, Janowiak J, Mo KC, Ropelewski C, Wang J, Leetmaa A, Reynolds R, Jenne R, Joseph D. 1996. The NCEP/NCAR 40-year reanalysis project. *Bulletin of the American Meteorological Society* 77:437–471. doi: [10.1175/1520-0477\(1996\)077<0437: TNYRP>2.0.CO;2](https://doi.org/10.1175/1520-0477(1996)077<0437: TNYRP>2.0.CO;2).
- Key RM, Kozyr A, Sabine CL, Lee K, Wanninkhof R, Bullister JL, Feely RA, Millero FJ, Mordy C, Peng T-H. 2004. A global ocean carbon climatology: results from Global Data Analysis Project (GLODAP). *Global Biogeochemical Cycles* 18: GB4031. doi: [10.1029/2004gb002247](https://doi.org/10.1029/2004gb002247).
- Kikata Y, Yonenobu H, Morishita F, Hattori Y. 1992. ^{14}C concentrations in tree stems. *Bulletin of the Nagoya University Furukawa Museum* 8:41–46. In Japanese.
- Kikata Y, Yonenobu H, Morishita F, Hattori Y, Marsoem SN. 1993. ^{14}C concentrations in tree stems I. *Mokuzai Gakkaishi* 39(3):333–337. In Japanese.
- Kohn MJ. 2010. Carbon isotope compositions of terrestrial C_3 plants as indicators of (paleo) ecology and (paleo)climate. *Proceedings of the National Academy of Sciences* 107: 19,691–19,695.
- Köhler P. 2016. Using the Suess effect on the stable carbon isotope to distinguish the future from the past in radiocarbon. *Environmental Research Letters* 11: 124016. doi: [10.1088/1748-9326/11/12/124016](https://doi.org/10.1088/1748-9326/11/12/124016).
- Krakauer NY, Randerson JT, Primeau FW, Gruber N, Menemenlis D. 2006. Carbon isotope evidence for the latitudinal distribution and wind speed dependence of the air-sea gas transfer velocity. *Tellus* 58B: 390–417. doi: [10.1111/j.1600-0889.2006.00223.x](https://doi.org/10.1111/j.1600-0889.2006.00223.x).
- Kudsk SGK, Olsen J, Nielsen LN, Fogtman-Schulz A, Knudsen MF, Karoff C. 2018. What is the carbon origin of early-wood? *Radiocarbon* 60(5):1457–1464. doi: [10.1017/RDC.2018.97](https://doi.org/10.1017/RDC.2018.97).
- Lehman SJ, Miller JB, Wolak C, Southon J, Tans PP, Montzka SA, Sweeney C, Andrews A, LaFranchi B, Guilderson TP, Turnbull JC. 2013. Allocation of terrestrial carbon sources using $^{14}\text{CO}_2$: methods, measurement, and modelling. *Radiocarbon* 55:1484–1495. doi: [10.1017/S0033822200048414](https://doi.org/10.1017/S0033822200048414).
- Lehman SJ, Miller JB. 2019. University of Colorado, Institute of Alpine and Arctic Research (INSTAAR), Radiocarbon Composition of Atmospheric Carbon Dioxide ($^{14}\text{CO}_2$) from the NOAA GML Carbon Cycle Cooperative Global Air Sampling Network, 2003–2018, Version: 2020–03–12.
- Levin I, Heshaimer V. 2000. Radiocarbon – a unique tracer of global carbon cycle dynamics. *Radiocarbon* 42(1):69–80.
- Levin I, Kromer B. 1997. Twenty years of atmospheric $^{14}\text{CO}_2$ observations at Schauinsland station, Germany. *Radiocarbon* 39(2):205–218.
- Levin I, Kromer B. 2004. The tropospheric $^{14}\text{CO}_2$ level in mid-latitudes of the Northern Hemisphere (1959–2003). *Radiocarbon* 46(3):1261–1272.
- Levin I, Kromer B, Francey RJ. 1996. Continuous measurements of ^{14}C in atmospheric CO_2 at Cape Grim. In: Francey RJ, Dick AL, Derek N, editors. *Baseline Atmospheric Program Australia 1994–1995*. Melbourne: CSIRO. p 106–107.
- Levin I, Kromer B, Francey RJ. 1999. Continuous measurements of ^{14}C in atmospheric CO_2 at Cape Grim, 1995–1996. In: Grass JL, Derek N, Tindale NW, Dick AL, editors. *Baseline Atmospheric Program Australia 1996*. Melbourne: Bureau of Meteorology and CSIRO Atmospheric Research. p. 89–90.
- Levin I, Naegler T, Kromer B, Diehl M, Francey RJ, Gomez-Pelaez AJ, Steele LP, Wagenbach D, Weller R, Worthy DE. 2010. Observations and

- modelling of the global distribution and long-term trend of atmospheric $^{14}\text{CO}_2$. *Tellus B* 62(1):26–46.
- Levin I, Kromer B, Schoch-Fischer H, Bruns M, Münnich M, Berdau D, Vogel JC, Münnich KO. 1985. 25 years of tropospheric ^{14}C observations in central Europe. *Radiocarbon* 27:1–19.
- Levin I, Kromer B, Steele LP, Porter LW. 2011. Continuous measurements of ^{14}C in atmospheric CO_2 at Cape Grim, 1997–2008. In: Derek N, Krummel PB, editors. *Baseline Atmospheric Program Australia 2007–2008*. Melbourne: Australian Bureau of Meteorology and CSIRO Marine and Atmospheric Research. p. 56–59.
- Libby WF. 1952. *Radiocarbon dating*. Chicago: University of Chicago Press.
- Libby WF. 1956. Radioactive fallout and radioactive strontium. *Science* 123(3199):657–660. doi: [10.1126/science.123.3199.657](https://doi.org/10.1126/science.123.3199.657).
- Manning MR, Lowe DC, Melhuish WH, Sparks RJ, Wallace G, Brenninkmeijer CAM, McGrill RC. 1990. The use of radiocarbon measurements in atmospheric studies. *Radiocarbon* 32(1):37–58.
- Marsh EJ, Bruno MC, Fritz SC, Baker P, Capriles JM, Hastorf CA. 2018. IntCal, SHCal, or a mixed curve? Choosing a ^{14}C calibration curve for archaeological and paleoenvironmental records from Tropical South America. *Radiocarbon* 60:925–940.
- Meijer HAJ, Pertuisot MH, van der Plicht J. 2006. High accuracy ^{14}C measurements for atmospheric CO_2 samples by AMS. *Radiocarbon* 48(3):355–372.
- Muraki Y, Kocharov G, Nishiyama T, Naruse Y, Murata T, Masuda K, Arslanov KhA. 1998. The new Nagoya radiocarbon laboratory. *Radiocarbon* 40(1):177–182.
- Murphy JO, Lawson EM, Fink D, Hotchkis MAC, Hua Q, Jacobsen GE, Smith AM, Tuniz C. 1997. ^{14}C AMS measurements of the bomb pulse in N- and S-hemisphere tropical trees. *Nuclear Instruments and Methods in Physics Research B* 123(1–4):447–450.
- Naegler T. 2009. Reconciliation of excess ^{14}C -constrained global CO_2 piston velocity estimates. *Tellus B* 61(2):372–384. doi: [10.1111/j.1600-0889.2008.00408.x](https://doi.org/10.1111/j.1600-0889.2008.00408.x).
- Naegler T, Levin I. 2006. Closing the global radiocarbon budget 1945–2005. *Journal of Geophysical Research* 111: D12311. doi: [10.1029/2005JD006758](https://doi.org/10.1029/2005JD006758).
- Nakamura T, Nakai N, Ohishi S. 1987a. Applications of environmental ^{14}C measured by AMS as a carbon tracer. *Nuclear Instruments and Methods in Physics Research B* 29(1–2):355–360.
- Nakamura T, Nakai N, Kimura M, Ohishi S, Hattori Y, Kikata Y. 1987b. Variations in ^{14}C concentrations of tree rings (1945–1983). *Chikyu-Kagaku (Geochemistry)* 21:7–12. In Japanese.
- Nydal R. 1968. Further investigation on the transfer of radiocarbon in nature. *Journal of Geophysical Research* 73(12):3617–3635.
- Nydal R, Gislefoss JS. 1996. Further application of bomb ^{14}C as a tracer in the atmosphere and ocean. *Radiocarbon* 38(3):389–406.
- Nydal R, Lövseth K. 1996. Carbon-14 measurement in atmospheric CO_2 from Northern and Southern Hemisphere sites, 1962–1993. Carbon Dioxide Information Analysis Center, World Data Center-A for Atmospheric Trace Gases, Oak Ridge National Laboratory, Tennessee.
- Oeschger H, Siegenthaler U, Schotterer U, Gugelmann A. 1975. A box diffusion model to study the carbon dioxide exchange in nature. *Tellus* 27(2):168–192.
- Olsson IU, Possnert G. 1992. ^{14}C Activity in different sections and chemical fractions of oak tree rings, AD 1938–1981. *Radiocarbon* 34(3):757–767.
- Park JH, Kim JC, Cheoun MK, Kim IC, Youn M, Liu YH, Kim ES. 2002. ^{14}C level at Mt Chiak and Mt Kyeryong in Korea. *Radiocarbon* 44(2):559–566.
- Pena-Ortiz C, Gallego D, Ribera P, Ordóñez P, Álvarez-Castro MDC. 2013. Observed trends in the global jet stream characteristics during the second half of the 20th century. *Journal of Geophysical Research: Atmospheres* 118:2702–2713. doi: [10.1002/jgrd.50305](https://doi.org/10.1002/jgrd.50305).
- Pickers PA, Manning AC. 2015. Investigating bias in the application of curve fitting programs to atmospheric time series. *Atmospheric Measurement Techniques* 8(3):1469–1489.
- Rafter TA, Ferguson GJ. 1957. “Atom bomb effect” – Recent increase of carbon-14 content of the atmosphere and biosphere. *Science* 126(3273):557–558. doi: [10.1126/science.126.3273.557](https://doi.org/10.1126/science.126.3273.557).
- Rakowski AZ, Nadeau M-J, Nakamura T, Pazdur A, Paweczyk S, Piotrowska N. 2013. Radiocarbon method in environmental monitoring of CO_2 emission. *Nuclear Instruments and Methods in Physics Research B* 294:503–507.
- Randerson JT, Enting IG, Schuur EAG, Caldeira K, Fung IY. 2002. Seasonal and latitudinal variability of troposphere $\Delta^{14}\text{CO}_2$: post bomb contributions from fossil fuels, oceans, the stratosphere, and the terrestrial biosphere. *Global Biogeochemical Cycles* 16(4):1112. doi: [10.1029/2002GB001876](https://doi.org/10.1029/2002GB001876).
- Reimer PJ, Brown TA, Reimer RW. 2004. Discussion: reporting and calibration of post-bomb ^{14}C data. *Radiocarbon* 46(3):1299–1304.
- Reimer PJ, Austin WEN, Bard E, Bayliss A, Blackwell PG, Bronk Ramsey CB, Butzin M, Cheng H, Edwards RL, Friedrich M, Grootes PM, Guilderson TP, Hajdas I, Heaton TJ, Hogg AG, Hughen KA, Kromer B, Manning SW, Muscheler R, Palmer JG, Pearson C, van der Plicht J, Reimer RW, Richards DA, Scott EM, Southon JR, Turney CSM, Wacker L,

- Adolphi F, Büntgen U, Capano M, Fahrni SM, Fogtmann-Schulz A, Friedrich R, Köhler P, Kudsk S, Miyake F, Olsen J, Reinig F, Sakamoto M, Sookdeo A, Talamo S. 2020. The IntCal20 Northern Hemisphere radiocarbon age calibration curve (0–55 cal kBP). *Radiocarbon* 62(4):725–757.
- Santini NS, Hua Q, Schmitz N, Lovelock CE. 2013. Radiocarbon dating and wood density chronologies of mangrove trees in arid Western Australia. *PloS ONE* 8(11):e80116. doi: [10.1371/journal.pone.0080116](https://doi.org/10.1371/journal.pone.0080116).
- Santos GM, Linares R, Lisi CS, Tomazello Filho M. 2015. Annual growth rings in a sample of Paran a pine (*Araucaria angustifolia*): toward improving the ^{14}C calibration curve for the Southern Hemisphere. *Quaternary Geochronology* 25:96–103. doi: [10.1016/j.quageo.2014.10.004](https://doi.org/10.1016/j.quageo.2014.10.004).
- Sierra CA. 2018. Forecasting atmospheric radiocarbon decline to pre-bomb values. *Radiocarbon* 60(4):1055–1066. doi: [10.1017/RDC.2018.33](https://doi.org/10.1017/RDC.2018.33).
- Speer JH. 2010. Fundamentals of tree-ring research. Tucson (AZ): University of Arizona Press. 368 p. ISBN 978-0-8165-2684-0.
- Stuiver M, Polach HA. 1977. Discussion: reporting of ^{14}C data. *Radiocarbon* 19(3):353–363.
- Stuiver M, Reimer PJ, Braziunas TF. 1998. Radiocarbon age calibration for terrestrial and marine samples. *Radiocarbon* 40(3):1127–1151.
- Suess HE. 1955. Radiocarbon concentration in modern wood. *Science* 122:415–417.
- Svarva H, Grootes P, Seiler M, Stene S, Thun T, Værnes E, Nadeau M-J. 2019. The 1953–1965 rise in atmospheric bomb ^{14}C in central Norway. *Radiocarbon* 61(6):1765–1774. doi: [10.1017/RDC.2019.98](https://doi.org/10.1017/RDC.2019.98).
- Tans P. 1981. A compilation of bomb ^{14}C data for use in global carbon model calculations. In: Bolin B, editor. *Carbon cycle modeling* (Scope 16). New York: John Wiley and Sons. p. 131–157.
- Telegadas K. 1971. The seasonal atmospheric distribution and inventories of excess carbon-14 from March 1955 to July 1969. U.S. Atomic Energy Commission Report HASL-243.
- Thoning KW, Tans PP, Komhyr WD. 1989. Atmospheric carbon dioxide at Mauna Loa Observatory 2, Analysis of the NOAA GMCC data, 1974–1985. *Journal of Geophysical Research* 94:8549–8563.
- Turnbull JC, Lehman SJ, Miller JB, Sparks RJ, Southon JR, Tans PP. 2007. A new high precision $^{14}\text{CO}_2$ time series for North American continental air. *Journal of Geophysical Research* 112:D11310. doi: [10.1029/2006JD008184](https://doi.org/10.1029/2006JD008184).
- Turnbull JC, Mikaloff Fletcher SE, Ansell I, Brailsford GW, Moss RC, Norris MW, Steinkamp K. 2017. Sixty years of radiocarbon dioxide measurements at Wellington, New Zealand: 1954–2014. *Atmospheric Chemistry and Physics* 17:14771–14784. doi: [10.5194/acp-17-14771-2017](https://doi.org/10.5194/acp-17-14771-2017).
- Turney CSM, Palmer J, Hogg A, Fogwill CJ, Jones RT, Bronk Ramsey C, Fenwick P, Grierson P, Wilmshurst J, O'Donnell A, Thomas ZA, Lipson M. 2016. Multidecadal variations in Southern Hemisphere atmospheric ^{14}C : Evidence against a Southern Ocean sink at the end of the Little Ice Age CO_2 anomaly. *Global Biogeochemical Cycles* 30:211–218. doi: [10.1002/2015GB005257](https://doi.org/10.1002/2015GB005257).
- Turney CSM, Palmer J, Maslin M, Hogg A, Fogwill CJ, Southon J, Fenwick P, Helle G, Wilmshurst J, McGlone M, Bronk Ramsey C, Thomas Z, Lipson M, Beaven B, Jones RT, Andrews O, Hua Q. 2018. Global peak in atmospheric radiocarbon defines the onset of Anthropocene Epoch in 1965. *Scientific Reports* 8:3293. doi: [10.1038/s41598-018-20970-5](https://doi.org/10.1038/s41598-018-20970-5).
- UNSCEAR. 2000. United Nations Scientific Committee on the Effects of Atomic Radiation UNSCEAR 2000 Report to the General Assembly, with Scientific Annexes volume I: Sources and Effects of Ionizing Radiation. https://www.unscear.org/docs/publications/2000/UNSCEAR_2000_Report_Vol.I.pdf
- Vogel JC, Marais M. 1971. Pretoria radiocarbon dates I. *Radiocarbon* 13(2):378–394.
- Vuille M, Burns SJ, Taylor BL, Cruz FW, Bird BW, Abbott MB, Kanner LC, Cheng H, Novello VF. 2012. A review of the South American monsoon history as recorded in stable isotopic proxies over the past two millennia. *Climate of the Past* 8: 1309–1321. doi: [10.5194/cp-8-1309-2012](https://doi.org/10.5194/cp-8-1309-2012)
- Willkomm H, Erlenkeuser H. 1968. University of Kiel radiocarbon measurements III. *Radiocarbon* 10(2):328–332.
- Xu S, Cook GT, Cresswell AJ, Dunbar E, Freeman SPHT, Hastie H, Hou X, Jacobsson P, Naysmith P, Sanderson DCW. 2015. Radiocarbon concentration in modern tree rings from Fukushima, Japan. *Journal of Environmental Radioactivity* 146:67–72. doi: [10.1016/j.jenvrad.2015.04.004](https://doi.org/10.1016/j.jenvrad.2015.04.004).
- Wu Y, Fallon S J, Cantin NE, Lough J M. 2021. Surface ocean radiocarbon from a Porites coral record in the Great Barrier Reef: 1945–2017. *Radiocarbon* 63(4):1193–1203. doi: [10.1017/RDC.2020.141](https://doi.org/10.1017/RDC.2020.141).
- Yamada Y, Yasuie K, Komura K. 2005. Temporal variation of carbon-14 concentration in tree-ring cellulose for the recent 50 years. *Journal of Nuclear and Radiochemical Sciences* 6(2):135–138.
- Yeloff D, Bennett KD, Blaauw M, Mauquoy D, Sillasoo Ü, van der Plicht J, van Geel B. 2006. High precision ^{14}C dating of Holocene peat deposits: a comparison of Bayesian calibration and wiggle-matching approaches. *Quaternary Geochronology* 1:222–235.

Zimnoch M, Jelen D, Galkowski M, Kuc T, Necki J, Chmura L, Gorczyca Z, Jasek A, Rozanski K. 2012. Partitioning of atmospheric carbon dioxide over Central Europe: insights from

combined measurements of CO_2 mixing ratios and their carbon isotope composition. *Isotopes in Environmental and Health Studies* 48(3): 421–433.

APPENDIX

Our compiled monthly data sets end at 2019.375 (Supplementary Table S2a–e), meaning that dating of organic samples formed after this time cannot be carried out reliably using these data. However, if the compiled data are extended to the more recent time by extrapolating, age estimation of the above samples can be performed.

We tried to fit the compiled monthly data sets for the NH zones from the 1980s onwards using an exponential trendline and employed it to extend the data beyond 2019. The best fit or highest R^2 value of the exponential trendline ($y = ae^{bx}$, with $a = 7112.837567 \pm 0.039233$ and $b = -0.004389 \pm 0.000020$) was achieved when the period of 1993–2019 was used. For the SH zones, the best fit was achieved when the period of 1994–2019 was employed. The constant parameters associated with the exponential trendline for the SH zones are $a = 4271.928748 \pm 0.034939$ and $b = -0.004132 \pm 0.000017$.

These exponential trendlines are recommended for use in extrapolating the zonal monthly data sets of the current compilation to no more than 5 years after 2019 for age estimation due to uncertain future emissions of fossil fuels (e.g., Graven 2015; Köhler 2016). However, users of these data should be aware that age estimation beyond the currently compiled data sets is considered as qualitative age approximation. Accurate age determination of organic samples formed after 2019 can only be achieved when a future compilation of atmospheric $\Delta^{14}\text{C}$ data extended beyond 2019 is available, probably in several years from now.